Ultrasound-Induced Ordering in Poly(3-hexylthiophene): Role of Molecular and Process Parameters on Morphology and Charge Transport

Avishek R. Aiyar,[†] Jung-Il Hong,[‡] Jessica Izumi,[§] Dalsu Choi,[†] Nabil Kleinhenz,[#] and Elsa Reichmanis*[†,⊥,#]

[†]Schools of Chemical and Biomolecular Engineering, [⊥]Materials Science and Engineering, [#]Chemistry and Biochemistry, Georgia Institute of Technology, Atlanta, Georgia 30332, United States

[‡]Department of Emerging Materials Science, DGIST, Daegu, Korea

[§]School of Chemical and Biochemical Engineering, University of Maryland, Baltimore County, Baltimore, Maryland 21250, United States

Ⓢ *Supporting Information*

ABSTRACT: Facile methods for controlling the microstructure of polymeric semiconductors are critical to the success of large area flexible electronics. Here we explore ultrasonic irradiation of solutions of poly(3-hexylthiophene) (P3HT) as a simple route to creating ordered molecular aggregates that result in a one to two order of magnitude improvement in field effect mobility. A detailed investigation of the ultrasound induced phenomenon, including the role of solvent, polymer regioregularity (RR) and film deposition method, is conducted. Absorption spectroscopy reveals that the development of low energy vibronic features is dependent on both the regioregularity as well as the solvent, with the latter especially influential on the intensity and shape of the band. Use of either higher regioregular polymer or ultrasonic irradiation of lower regioregular polymer solutions results in high field effect mobilities that are nearly independent of the dynamics of the film formation process. Surprisingly, no distinct correlation between thin-film morphology and macroscopic charge transport could be ascertained. The relationships between molecular and process parameters are very subtle: modulation of one effects changes in the others, which in turn impact charge transport on the macroscale. Our results provide insight into the degree of control that is required for the development of reproducible, robust materials and processes for advanced flexible electronics based on polymeric materials.

KEYWORDS: *polymer semiconductor, poly(3-hexylthiophene), ultrasonication, morphology, charge transport, nanofibrils, OFETs*
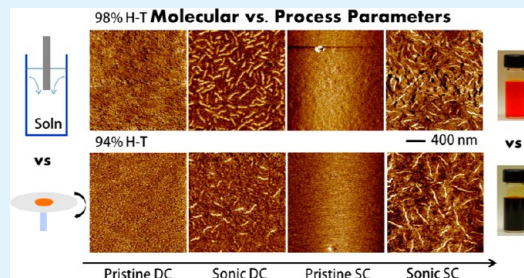
■ INTRODUCTION

Polymeric semiconductors are emerging as potential competitors to amorphous silicon, with field effect mobilities now approaching 2 cm^2 V^{-1} s^{-1}.[1] Such advances are crucial to sustaining the development of "macroelectronics" as a commercially viable technology for applications such as organic solar cells, light-emitting diodes (OLEDs), and field-effect transistors (OFETs).[2,3] The conjugated polymers that form the basis for these applications must possess thin film morphologies that are favorable towards charge transport. This requirement has stimulated the need to further our understanding of thin film morphology at the nano- through microstructural regimes in order to develop charge-transport correlations, especially because the morphology of polymeric thin films can encompass a wide range of structures ranging from largely amorphous to ones that exhibit highly ordered crystalline domains.[4−9]

Regioregular poly(3-hexylthiophene) (P3HT) is a readily accessible high mobility polymer,[8,10] that is an effective model for understanding the impact of microstructure on charge transport.[11−13] P3HT has allowed elucidation of both intrinsic and extrinsic factors that influence the morphology and microstructure of resultant thin films and concomitantly, macroscopic charge transport. Intrinsic molecular based parameters such as regioregularity (RR) of side chain attachment[11] and molecular weight[5] have emerged as key metrics that control polymer thin film architecture. However, in addition to those intrinsic molecular features, extrinsic factors involving parameters such as film deposition method,[13] solvent,[6,14] polymer-dielectric interface treatment,[8,15] and thermal annealing[16,17] that are associated with thin film and thus device preparation, have also been identified as pertinent to attaining morphologies favorable for efficient charge transport in π-conjugated materials, and as a consequence, optimum device performance.

Although the importance of polymer thin film microstructure has been recognized, there is currently no consensus as to its exact role in influencing charge transport. Highly crystalline architectures exhibiting enhanced π- stacking between the conjugated backbones are expected to effect increased electronic coupling, which in turn promotes polaron delocalization over larger length scales.[18] Thus, high crystallinity has been viewed as vital for achieving effective macroscopic charge transport. However, Kline, et al. demonstrated that amorphous, high molecular weight P3HT films routinely exhibit mobilities that are several orders of magnitude higher than those obtained with crystalline films attained with a low molecular weight variant.[5] In addition, the dependence of transport properties on the processing history of the thin film can result in a large variation in the mobility of nominally the same material.[6−8,19] Polymeric systems are inherently structurally heterogeneous, characterized by the coexistence of ordered as well as disordered phases,[20,21] which makes microstructure−-charge transport correlations nontrivial. Nevertheless, simultaneous consideration of intrinsic as well as extrinsic factors is expected to elucidate these correlations, and valuable insights that will aid the design of the next generation of conjugated polymers are envisaged.

Ultrasonic irradiation of P3HT solutions in chloroform ($CHCl_3$) has been reported to lead to the formation of ordered precursors in the solution that survive a spin-casting process, and are manifest in the solid state as nanofibrillar structures.[9] The field effect mobilities of such spin-cast films exhibit a dramatic two order of magnitude increase over non-irradiated analogs.[9] Ultrasonic irradiation was shown to be a useful tool for inducing a tunable crystallinity in resultant thin films that proved invaluable in identifying a percolation type charge transport mechanism operating in the P3HT OFETs studied. However, the impact of polymer molecular characteristics, RR being of prime interest, and the role of solvent choice and processing conditions such as film deposition method on the ultrasonication process has not been assessed.

Here it is demonstrated that although π-stacked aggregates can be induced in P3HT solution prior to thin film formation, the ultrasound induced aggregation process is sensitive to both polymer RR and solvent, and importantly, extrinsic factors such as the film deposition method can have a substantial impact on the final morphology of resultant P3HT films. We systematically explore the roles of polymer RR and solvent in regulating the aggregation process, and investigate their corresponding impact on thin film morphology and charge transport characteristics. The field-effect mobilities obtained from polymers having different RRs (ca. 94% and >98%) and prepared using a diverse set of processing conditions vary by roughly 1 order of magnitude, and are not commensurate with observed variations in the corresponding thin-film morphologies. No distinct correlation between thin-film morphology and macroscopic charge transport could be ascertained. We suggest that the dependence of π-conjugated polymer film morphology on both intrinsic (RR) and extrinsic (film deposition method and solvent) factors provides vital insight into parameters that must be carefully considered in order to achieve optimized morphologies that support facile charge transport in polymeric semiconductors.

■ EXPERIMENTAL METHODS

Materials. Regioregular P3HT (referred to as HT94 and HT98 henceforth) was purchased from Sigma Aldrich (catalog no. 445703)

and Rieke Metals Inc. (P200 Sepiolid), respectively, and used without further purification. The molecular weight and regioregularity of both samples are summarized in Table 1. The primary solvents used in this

Table 1. Molecular Weight and Regioregularity of the P3HT Samples Used

P3HT sample	mol wt (kDa)		regioregularity (%HT)
	M_n	M_w	
HT94	24	47.7	ca. 94
HT98	12.7	23	>98

study were anhydrous grade, purchased from Sigma Aldrich, and used without further purification. Trichloro(octadecyl)silane (OTS) and hexamethyldisilazane (HMDS) were also purchased from Sigma-Aldrich and used without further purification.

The MW data were obtained through gel permeation chromatography (GPC) of the polymer samples in tetrahydrofuran solution. A Waters 1515 Isocratic high-performance liquid chromatography system with a Waters 2489 UV/vis detector fitted with a Styragel HR 5E column was used. MW data were determined using polystyrene standards. Polymer regioregularity was estimated from the ^1H NMR spectra obtained from deuterated chloroform solution at 293 K using a Bruker DSX 300.

Organic FET (OFET) Fabrication and Characterization. The FET devices used for electrical characterization consisted of two contact devices where P3HT films were prepared via spin-coating the relevant polymer solution onto either a 200 or 300 nm thick SiO_2 gate dielectric. The highly doped silicon wafer served as the gate electrode while Au/Cr was used for the source and drain contacts. The source and drain contacts were fabricated using a standard photolithography based lift-off process, followed by E-beam evaporation (CVC Inc.) of 50 nm Au contacts with 5 nm of Cr as the adhesion layer. Before spin-coating P3HT solutions, the dielectric surface was cleaned using one of two processes: (i) cleaning the substrates in piranha solution (4 parts sulfuric acid:1 part hydrogen peroxide) followed by cleaning with acetone, isopropanol, and deionized water in an ultrasound cleaning bath, or (ii) placing the devices in a UV-Ozone cleaner (Novascan PSD-UV) 15 min. Both (i) and (ii) allow for complete removal of any residual photoresist and other organic contaminants. The substrates were rendered hydrophilic at the end of either treatment, although UV-Ozone cleaning appears to result in a lower contact angle as determined by a visual examination.

Solutions of P3HT were prepared at a concentration of ca. 3−4 mg/mL by heating the solution on a contact hot-plate at a temperature close to the boiling point of the solvent used (e.g., at 55 °C for chloroform ($CHCl_3$) as the solvent). A table-top ultrasonic cleaner (Bransonic 2510, 40 kHz, 130 W) was used for ultrasonic irradiation of the solutions. The solutions were prepared and ultrasonicated in sealed glass vials to prevent solvent evaporation. Ultrasonic irradiation was performed by first sealing the capped glass vials with paraffin paper and then removing the vials from a nitrogen filled glovebox temporarily, ultrasonicated and then replaced inside the box. OFETs were prepared by either dip-coating (DC) or spin-coating (SC) the solutions onto the precleaned substrates and tested using an Agilent 4155C semiconductor parameter analyzer. The field effect mobility was calculated in the linear region of transistor operation ($V_D = -3$ V) by plotting the drain current (I_D) versus the gate voltage (V_G) and fitting the data to the following equation[22]

$$I_D = \mu C_{ox} \frac{W}{L} (V_G - V_T) V_D$$

Where V_T is the threshold voltage, W and L are the transistor channel width and length respectively and C_{ox} is the capacitance per unit area of the silicon dioxide gate dielectric = 1.72×10^{-8} F cm^{-2} (for 200 nm thick oxide) or 1.15×10^{-8} F cm^{-2} (for 300 nm thick oxide). For spin-coating, the substrates were spun at a speed of 1500 rpm that resulted in ca. 25−30 nm thick polymer films (as determined by spectroscopic ellipsometry). Dip-coating was performed manually by lowering the

substrates vertically into the stock solution of the polymer in CHCl₃, where it was allowed to sit (again vertically) for a period of 1 min before slowly withdrawing the substrate vertically, resulting in films that were ca. 20 nm thick. Because the entire operation was conducted manually, some variations in the morphology and possible charge transport are expected as will be discussed below. Both spin-coated and dip-coated films were then thermally annealed at 110 °C for 10 h on a contact hot plate inside a nitrogen-filled glovebox. It must be noted that there are variations in ultrasound intensity across the ultrasound bath and therefore between experiments that can complicate the results, especially in the absence of quantification of the ultrasound intensity. However, we have tried to account for such variations. Unless otherwise mentioned, all experiments were performed in a nitrogen filled glovebox with less than 1 ppm of oxygen and moisture.

UV–Vis Spectra of P3HT. The solid-state UV–vis spectra were obtained using an Agilent 8510 Spectrophotometer by spin-coating the P3HT solutions onto precleaned glass slides under conditions equivalent to those for OFET fabrication.

Grazing Incidence X-ray Diffraction Studies. Out-of-plane (OOP) grazing incidence X-ray diffraction data were obtained using a Panalytical X'Pert Pro system equipped with a Cu X-ray source operating at 45 kV and 40 mA. Grazing incidence angle was fixed at 1° and the detector was scanned from 3 to 20°. Peak positions were obtained from the measured profiles by fitting the peaks using XRD analysis software (MDI JADE). Samples for GIXD measurements were prepared by spin-coating P3HT solutions onto hydrophilic silicon substrates having a native oxide that were cleaned using the same procedure used for bottom contact FET structures. The solutions used for the GIXD measurements were as the identical solutions used for OFET measurements.

Atomic Force Microscopy (AFM) studies of P3HT. AFM measurements were performed on films prepared by spin-coating the P3HT solutions onto bare silicon dioxide substrates prepared under the same conditions as the bottom contact OFET substrates with a Veeco Digital Instruments Dimension 3100 scanning probe microscope in tapping mode with a silicon tip (NSC 14, Mikromasch).

RESULTS AND DISCUSSION

In separate studies, it has been noted that both polymer regioregularity and process parameters associated with film formation/preparation influence thin film microstructure, and thus charge transport.[10,11,13,18,23] The field effect mobilities obtained from HT94 and HT98 P3HT (lower and higher RR material, respectively) OFETs fabricated by either spin-casting or dip-coating from pristine as well as ultrasonicated CHCl₃ solutions of the polymer are shown in Figure 1(a). Numerical values of the field effect mobility obtained under the scenarios investigated here are enumerated in Table II. Because P3HT RR impacts the susceptibility of the material to ultrasonic irradiation (vide infra), HT94 P3HT solutions were irradiated for ca. 10 min, whereas HT98 solutions were irradiated for only ca. 5 min. The mobility of HT94 P3HT OFETs varies by more than one order of magnitude for spin-coated films obtained from pristine solutions vs dip-coated films obtained from the ultrasonicated variant respectively. In contrast, the calculated mobility for devices prepared with the higher RR material, HT98 P3HT, differed by only a factor of about 3 for films obtained by spin-coating from the pristine and ultrasonicated CHCl₃ solutions, respectively. It is a combination of both differences in polymer regioregularity as well as processing conditions that lead to differences in the observed mobilities. However, the precise impact of each variable is not clearly discerned.

Figures 1b, 2a, and 2b display representative transfer and output characteristics of HT94 P3HT devices obtained from
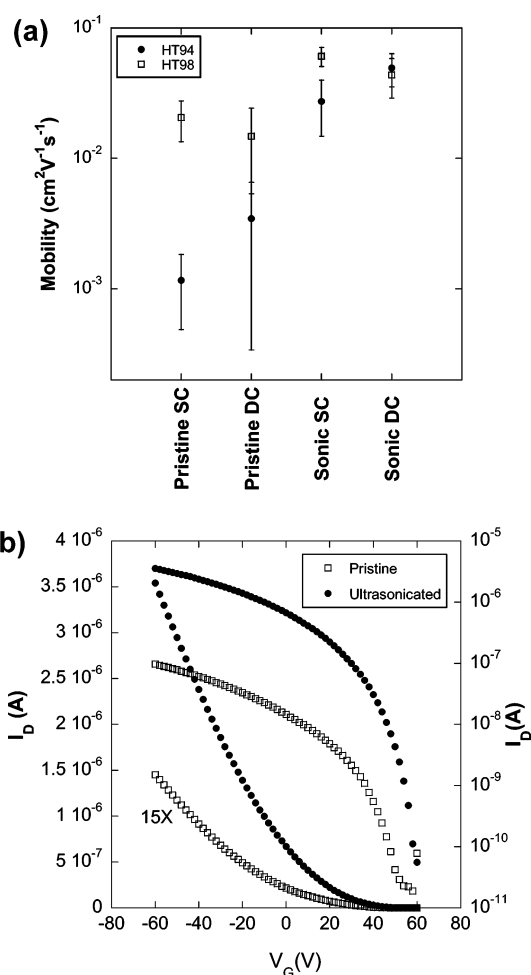

Figure 1. (a) Effect of processing conditions on mobility of films obtained by ultrasonic irradiation of P3HT solutions. All experiments conducted inside a glovebox. (b) Representative transfer characteristics obtained from HT94 P3HT films spin-coated from pristine as well as ultrasonicated solutions in CHCl₃. All the devices were thermally annealed in a nitrogen glovebox for a period of ca. 10 h.

Table II. Field Effect Mobilities Obtained from HT94 and HT98 OFETs Obtained under Different Conditions

condition	HT94 Mobility $(cm^2V^{-1}s^{-1})$	HT98 Mobility $(cm^2V^{-1}s^{-1})$
pristine SC	$1.16 \pm 0.67 \times 10^{-3}$	$2.05 \pm 0.71 \times 10^{-2}$
pristine DC	$3.45 \pm 3.11 \times 10^{-3}$	$1.48 \pm 0.95 \times 10^{-2}$
ultrasonicated SC	$2.73 \pm 1.25 \times 10^{-2}$	$6.08 \pm 1.01 \times 10^{-2}$
ultrasonicated DC	$4.94 \pm 1.41 \times 10^{-2}$	$4.36 \pm 1.46 \times 10^{-2}$

the pristine and ultrasonicated CHCl₃ solutions, which are typical of p-channel OFET operation in the accumulation mode. The high turn-on voltages (V_{ON}) (see Figure 1b) are attributed to the effects of residual doping and/or acceptor-like traps at the P3HT-oxide interface.[24,25] Such effects are especially likely given the absence of passivation of hydroxyl groups (generated because of the piranha/UV-ozone treatment of the substrates) that can act as charge traps.[26] Additional experiments confirm that there is indeed a large reduction in V_{ON} when using semiconductor-dielectric modifications (see the Supporting Information). While further investigation into this phenomenon is warranted, a detailed study of the effects of semiconductor–dielectric interface modification on the mor-

2370

dx.doi.org/10.1021/am3027822 | ACS Appl. Mater. Interfaces 2013, 5, 2368–2377
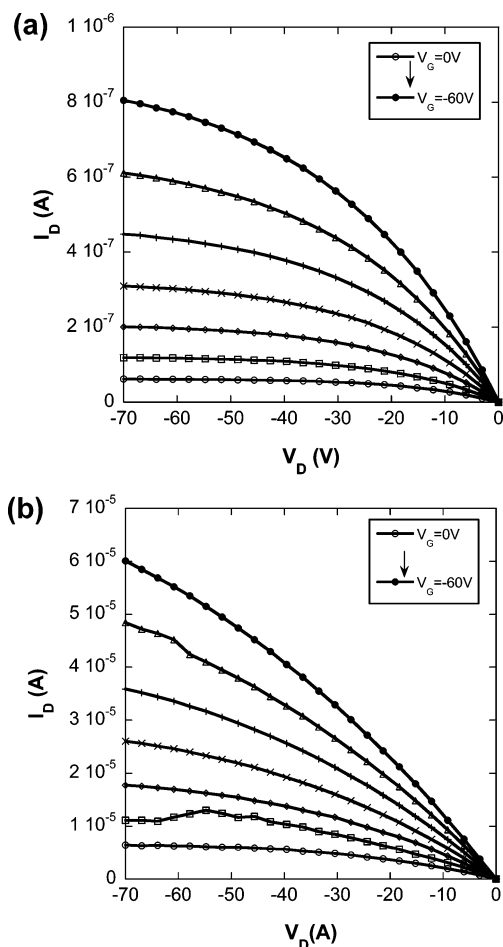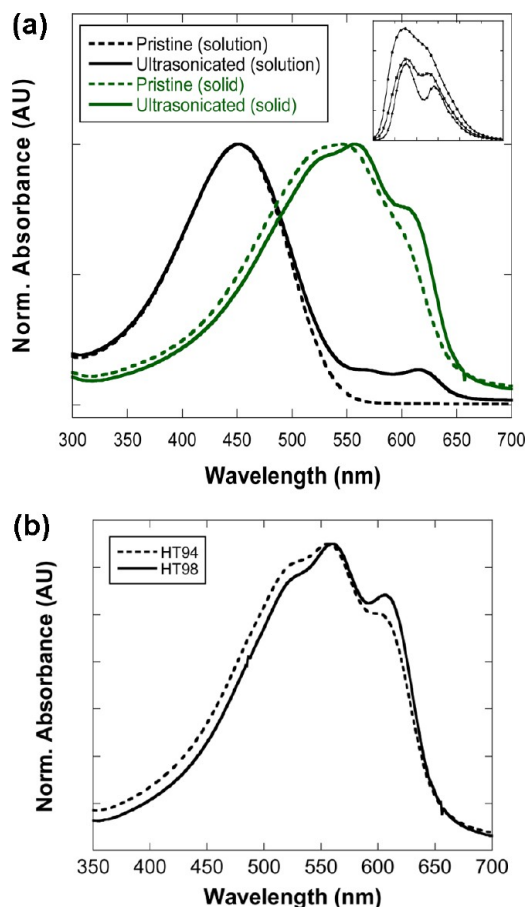
Figure 2. Representative output characteristics obtained from HT94 P3HT films obtained by spin-coating from (a) pristine and (b) ultrasonicated solutions in CHCl₃.

UV−visible absorption spectral features strongly correlate with the state of structural order in π-conjugated polymer films.[30−32] The spectroscopic changes observed upon ultrasonic irradiation of the P3HT solutions investigated here are summarized in Figure 3a, where the development of the low

Figure 3. (a) Normalized solution and solid state UV−vis plots for pristine and ultrasonicated HT94 P3HT/CHCl₃ solutions. Inset shows the solution photoluminescence spectra of pristine, 5 min ultra-sonicated and 10 vol.% MeOH aggregated P3HT/CHCl₃ solutions. (b) Comparison of absorption spectra of HT94 P3HT and HT98 P3HT films obtained from ultrasonicated solutions. All solutions ultrasonicated for ca. 5 min.

phology and charge transport in P3HT was not conducted here.

The effect of process parameters on charge carrier transport is significantly more apparent for lower RR P3HT (HT94). A comparison of the HT94 P3HT OFET mobilities achieved using dip-coating vs spin-casting demonstrates that the former routinely affords films that exhibit higher mobilities. Dip-coating may facilitate formation of films with near-equilibrium structures and higher crystallinity.[27,28] For the higher RR HT98 material, the correlation is reversed: spin-coating leads to films exhibiting higher mobilities. These trends provide evidence of an interplay between polymer molecular properties and process oriented effects, both of which are important in determining the final semiconducting film morphology.[11] The subtle effects of RR on the morphology as well as charge transport in spin-coated P3HT films was recently documented, and the results presented here further demonstrate those effects. Given that charge transport in field effect transistors is dominated by an accumulation layer that only spans a few monolayers from the polymer-dielectric interface,[29] the ordering of the macro-molecules at that interface is expected to exert a dominating influence on charge carrier mobility. Thus, the differences in mobility noted between both dip-coated and spin-coated films, as well as between HT94 and HT98 films, most likely originate from the thin film nano- through microstructures.

energy features in the solution (at ca. 570 and 620 nm) and solid state spectra (at ca. 605 nm) is associated with the presence of crystalline aggregates in solution that in turn provide for increased molecular order in the solid films.[9] In addition, compared to the corresponding pristine HT94 P3HT solutions, the intensity of photoluminescence (inset of Figure 3a) decreases by 47 and 36% upon either ultrasonic irradiation or addition of 10 vol % methanol respectively, consistent with the formation of a π-stacked aggregate that can partially quench polymer luminescence.[33,34]

Zhao et.al. suggested that the primary effect of ultrasonic irradiation of a P3HT solution is a dramatic increase in interaction between the solute (individual polymer chains) and the solvent, resulting in decreased chain entanglement, which in turn promotes polymer−polymer association.[35] Thus, this disorder−order transformation is expected to be influenced by the conformation of the individual polymer chains, and molecular parameters such as RR are expected to impact the

effects of ultrasonic irradiation. The solid state absorption spectra of HT94 and HT98 P3HT films obtained from the respective ultrasonically irradiated solutions are shown in Figure 3(b). A bathochromic shift of the absorption maximum λ_{max} from 556 nm for the HT94 film to 561 nm for the HT98 film is observed. The latter also shows a more pronounced shoulder at ca. 602 nm. The increased intensity of the (0−0) transition (and thus of the intensity ratio of the (0−0) and (0−1) transitions) in the HT98 film is indicative of increased intermolecular ordering in the higher RR film, and is likely to arise from an extended main chain conformation afforded by fewer steric distortions.[30,32] The enhanced intrachain ordering is also reflected in the lower free exciton bandwidth in the HT98 vs HT94 film (ca. 57 meV in HT98 vs ca. 88 meV in HT94, see the Supporting Information).[31]

The UV−vis spectroscopic results demonstrate the dependence of the ultrasound induced aggregation process on polymer RR, and is consistent with the extent of intrachain order being extremely sensitive to subtle changes in the head−tail (HT) attachments of the alkyl side chains. On the basis of the results of Wang et.al., similar differences in the absorption spectra are also expected between spin- vs dip-coated films, with the latter yielding films with higher molecular order.[36] Taking all of the spectral data into account, increased intermolecular ordering associated with films of HT98 P3HT may explain the higher mobility obtained for the higher RR material. Ultrasonic irradiation of P3HT solutions (regardless of RR) results in changes to the absorption spectra that bear remarkable similarities to the effect of RR alone (in the absence of any ultrasonic irradiation), which implies that the ultrasound-induced increase in mobility shares a common origin with that of RR, namely, increased molecular order.

P3HT thin film morphology differences are apparent in the tapping mode AFM phase images shown in Figure 4. Spin-
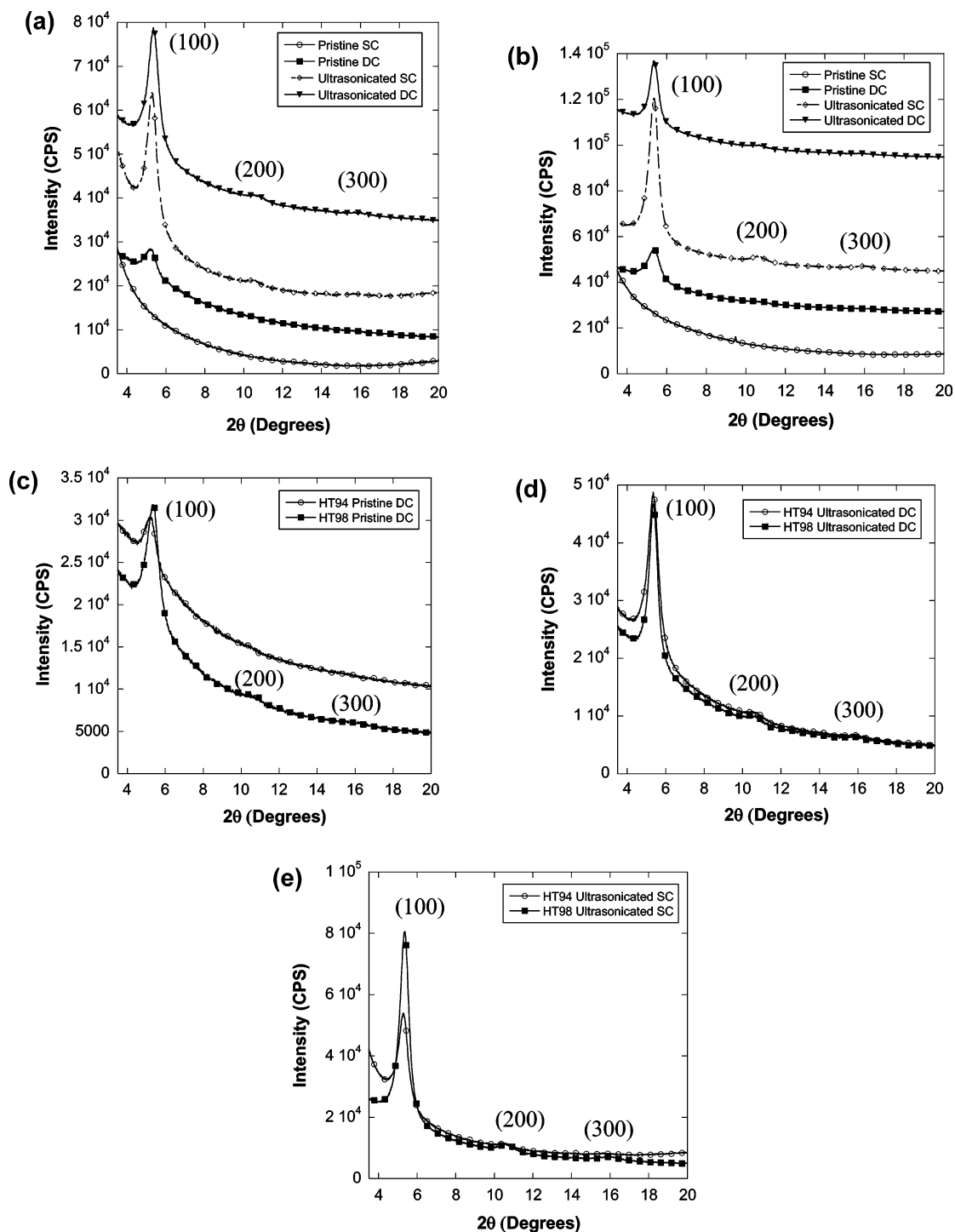

HT98

HT94   — 400 nm

| Pristine DC | Sonic DC | Pristine SC | Sonic SC |
| (a) | (b) | (c) | (d) |
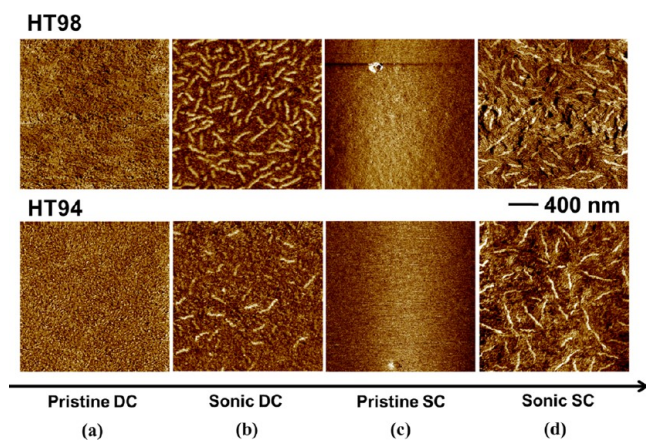
Figure 4. Tapping mode AFM phase images of HT94 and HT98 P3HT films obtained by spin-coating as as well dip-coating from pristine as well as ultrasonicated CHCl$_3$ solutions.

coated films of both HT94 as well as HT98 P3HT obtained from pristine solutions appear relatively featureless and lack texture, Figure 4c. This observation is consistent with the rapid drying times encountered in spin-coating from volatile solvents such as CHCl$_3$, resulting in a kinetically limited process that suppresses the formation of ordered structures.[6] The absence of ordered structures in the AFM phase images is mirrored in the X-ray diffractograms, Figure 5, where no discernible peak was detected for either film obtained from a spin-coated pristine

solution. Spin-coated films of HT94 P3HT routinely exhibit mobilities that are the lowest in magnitude ($\mu = 1.16 \pm 0.67 \times 10^{-3}$ cm^2 V^{-1} s^{-1}, HT94). While the film morphologies for spin-coated solutions of pristine HT98 P3HT display no obvious signs of order, HT98 mobility is about one order of magnitude higher, $2.05 \pm 0.71 \times 10^{-2}$ cm^2 V^{-1} s^{-1}. Interestingly, a dip-coating process results in film morphologies that clearly incorporate nanofibrillar structures in both P3HT samples, both with and without ultrasonication of the respective solutions, Figure 4a. The higher mobility of dip-coated films obtained from pristine HT94 P3HT solutions indicates that the presence of the nanofibrillar network is representative of increased structural order, which in turn promotes more facile charge transport.

Although not direct evidence for the presence of structural order, the nanofibrils are a strong indication of π−π associations between adjacent polymer chains that are a prerequisite for, and result in, their formation.[37] A similar nanofibrillar network is visible in dip-coated HT98 P3HT films obtained from pristine solutions, even though, surprisingly, the mobilities are slightly lower or comparable to those obtained via the spin-coating process where nanofiber formation is significantly suppressed. Further, spin-coated films of HT98 have a mobility that is almost 1 order of magnitude higher than that obtained from devices prepared with dip-coated lower RR, HT94, even though HT94 films exhibit a distinct nanofibrillar network. These results are also reflective of the molecular weight dependence of charge transport in P3HT reported by others, demonstrating that a highly ordered nano/micro-structure may not necessarily provide for high charge carrier mobilities.[5] We note that although the development of the nanofibrils themselves is a nanoscale phenomenon, given the macroscopic nature of the charge transport in OFETs, we focus our attention on the "micro"-structure of the films incorporating these nanofibrils.

The (100) peak in the X-ray diffractograms, associated with the lamellar packing of polymer chains along the crystallographic direction perpendicular to the backbone,[38] which was clearly absent in the spin-coated films, appears well-developed in dip-coated films of both the higher and lower RR sample, although the peak is more intense for the HT98 film. The development of the (100) peak for materials deposited via dip-coating confirms the formation of "near-equilibrium" ordered structures, which are otherwise quenched when deposition is effected via spin-coating.[27,28] The X-ray peak intensities are consistent with the improvement in the mobility observed for dip-coated HT94 films and could explain the difference in mobility noted between HT94 and HT98 dip-coated films, but it fails to account for the demonstrated differences in mobility of the spin-coated films for which the (100) peak is noticeably absent. Rather, the higher degree of intrachain ordering afforded by the higher RR in HT98 may compensate for the kinetically hindered structures that emanate upon spin-coating, thus perhaps counterbalancing a decreased level of interchain order and preventing mobility from being compromised as a result of the observed disordered morphology (AFM and XRD analysis). Therefore, the higher macroscopic mobility demonstrated for spin-coated HT98 films may be the result of reduced reorganization energies that allow for facile interchain hopping in spite of the absence of nanofibrillar structures.[39] This supposition finds support in the absorption spectra of P3HT films, where subtle variations in the RR result in increased molecular order in the films.

Figure 5. Grazing incidence X-ray diffraction profiles of (a) HT94 and (b) HT98 P3HT films obtained by spin-coating and dip-coating from pristine and ultrasonically irradiation solutions in CHCl$_3$. Comparison of the XRD profiles of HT94 and HT98 films obtained by (c) dip-coating from pristine solutions, (d) dip-coating from irradiated solutions, and (e) spin-coating from irradiated solutions.

Ultrasonic irradiation of the P3HT solutions effects dramatic changes to the morphology as well as the (100) peak intensities, confirming observations of the impact of ultrasound on thin film microstructure.[9] The morphology of both spin- and dip-coated films of HT94 and HT98 P3HT obtained from the irradiated samples are characterized by the presence of distinct nanofibrillar structures embedded in a matrix that is composed of both disordered and quasi-ordered structures.[9] Although the ordered precursors are thought to be generated in solution, the film deposition method and the polymer RR influence their manifestation in the solid state, images b and d in Figure 4. For example, a comparison of films obtained by dip- vs spin-coating reveals subtle differences in the physical attributes of the nanofibrillar structures incorporated into both films. Additionally, the effect of RR is clearly apparent upon dip-coating: the HT94 film contains a significantly lower fraction of nanofibrillar structures compared to the HT98 counterpart. The same solutions were used for both the spin-

coating and dip-coating experiments to avoid ambiguities associated with changes in irradiation intensities noted in the Experimental Section. Also, the irradiation times required for HT94 and HT98 solutions were different; the lower RR variant was routinely less sensitive to ultrasound induced changes in comparison solutions of HT98 (vide infra).

In sharp contrast to the dip-coated films, a significantly smaller difference in the morphologies obtained from spin-coated films is noted, Figure 4d, suggesting that the differences observed for the dip-coated films arise predominantly from the deposition method itself, rather than any difference in ultrasonication time. The increase in the (100) peak intensity in the X-ray diffractograms for both spin-coated as well as dip-coated films is consistent with the appearance of ordered nanofibrillar structures within the film as a result of ultrasonic irradiation. The slightly higher (100) peak intensity for HT98 mirrors the AFM phase image, which detects the presence of a greater number of ordered nanofibrils relative to HT94 films, Figure 4d. However for dip-coated films, although the distribution of ordered nanofibrils in the HT94 film appears sparse relative to HT98, Figure 4b, the (100) X-ray peak intensities are near identical for both. The apparent identical crystallinity between the two samples may result from an equal overall distribution of disordered, quasi-ordered, and ordered phases. In the absence of any appreciable thickness difference between the two films (ca. 19 nm and ca. 21 nm for HT94 and HT98, respectively), the near identical (100) peak intensities point to the presence of a near equal volume fraction of ordered crystallites in both films. Thus, the lower fraction of ordered crystallites in the HT94 film may be compensated by a higher areal fraction of the quasi-ordered phase, and affords a net degree of crystallinity similar to that obtained from the higher RR sample, where the effect of a greater number of nanofibrillar structures is offset by a higher disordered amorphous content. Moreover, the different morphologies of dip-coated HT94 and HT98 films again highlight the delicate interplay between effects related to molecular structure (for instance, polymer RR) and the dynamics of film formation.

We have previously suggested that the formation of ordered nanofibrils involves sequential nucleation of π-stacked polymer aggregates into an intermediate quasi-ordered phase and eventually into the ordered phase.[9] This mechanism, coupled with the fact that HT98 P3HT is far more sensitive to ultrasonic irradiation, suggests a greater conversion of the intermediate quasi-ordered phase into an ordered phase providing for films that incorporate greater numbers of the nanofibrillar structures embedded within the remaining, largely disordered material. In contrast, the weaker response to ultrasonic irradiation of the lower RR polymers results in fewer ordered nanofibrils, but a greater conversion of the disordered phase into one which is quasi-ordered. In this scenario, the facile charge transport expected within the ordered nanofibrils in films of HT98 accessed through dip-coating is offset by poor transport within the amorphous matrix resulting in a macro-scale mobility of $4.36 \pm 1.46 \times 10^{-2}$ cm^2 V^{-1} s^{-1}, a value that is essentially identical to that obtained from HT94 dip-coated films, where the lower fraction of ordered nanofibrils is believed to be offset by a higher areal fraction of the quasi-ordered phase.

The variations in film crystallinity and morphology noted in Figures 4 and 5 are, however, insufficient to fully justify the differences in mobility observed in Figure 1. For example, the dramatic difference in the degree of crystallinity and the film morphology between HT94 films obtained by spin-coating from pristine versus ultrasonicated solutions adequately explain the increase in mobility ($1.16 \pm 0.67 \times 10^{-3}$ cm^2 V^{-1} s^{-1} to $2.73 \pm 1.25 \times 10^{-2}$ cm^2 V^{-1} s^{-1}) obtained from the corresponding films, however, similar differences in micro-structural properties observed for the higher RR HT98 films afford mobility differences that are incommensurate, differences of as little as a factor of 3 are observed. These results again highlight the importance of intra- vs inter-chain effects and their associated balance and interplay, in dominating macroscopic charge transport. The inherently higher intra-chain order in the highly RR HT98 films obtained from pristine solutions, evidenced by solid state absorption spectral data, provides a rationale for why only minor differences in mobility are obtained through ultrasonic irradiation in spite of a large increase in the degree of interchain ordering.

Interestingly, the mobility of HT98 P3HT films obtained by spin-coating irradiated solutions in CHCl$_3$ that had been filtered through a 0.2 μm filter, was only lower by a factor of 1.6 relative to nonfiltered solutions, in spite of the observed drastic reduction in the number of ordered nanofibrils, Figure 6. However, we note that in the case of the latter, i.e., films obtained from filtered solutions, the mobility remains higher than that obtained from pristine HT98 solutions by a factor of 4. Although there is a reduction in the ordered nanofibril content of the film, there is a higher degree of order relative to the films obtained from pristine solutions, Figures 6b and 4a. The reduction in nanofibril content obtained upon ultra-sonication is mirrored in the UV–vis spectra, which show a decrease in the concentration of "crystallized" aggregates in solution (see the Supporting Information). This result is consistent with a percolation type charge transport mechanism, where any increase in the nano/microstructural quality of the film beyond a percolation threshold will not necessarily result in further improvement in macroscopic charge transport, especially when the charges encounter large-area amorphous or quasi-ordered regions.[9]
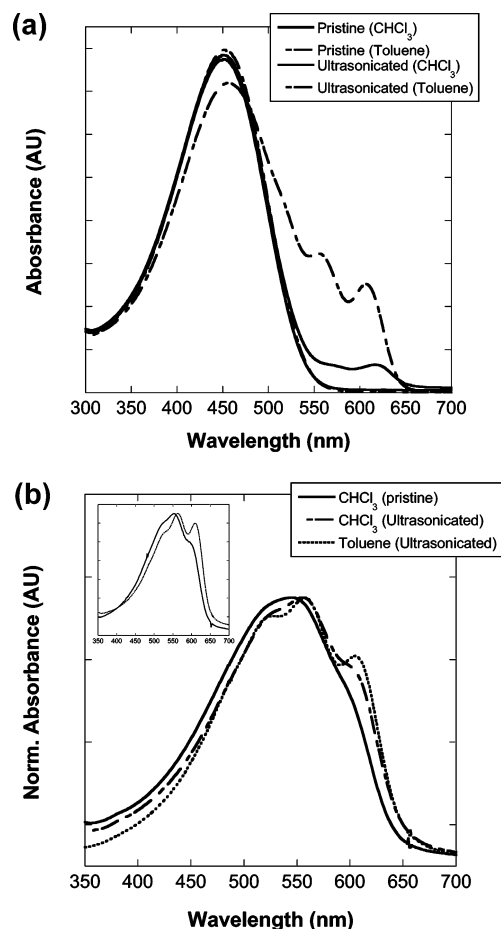
In spite of the role played by film deposition conditions, it is evident that intrinsic molecular properties such as the RR are crucial to the manifestation of the ultrasound induced phenomenon reported here and elsewhere.[9,35] As hypothesized by Zhao et al., changes observed upon ultrasonic irradiation are fundamentally ones of disorder–order transitions.[35] It is additionally suggested that the acoustic cavitation process present during ultrasonication leads to chain disentanglement followed a shear induced change of the polymer chain conformation resulting in maximized opportunities for cofacial stacking between individual polymer chains.[9] Thus, the nature of the molecular aggregate formed will depend upon the solvent environment surrounding the disentangled chains prior to π–π association. Elucidation of the role of solvent–solute interactions in general is expected to clarify understanding of the molecular aggregation process that results from ultrasonic irradiation. Through experiments with P3HT of varying molecular weights (M_w = 11, 30–40, and 87 kDa), Zhao et al. suggested that the effects of ultrasonic irradiation are reduced to that of solubility of the polymer in the solvent system.[35] In their experiments, the disorder–order trans-formations in high molecular weight P3HT/xylene solutions were significantly more favorable relative to medium and low MW polymer solutions. Their results were mirrored not only in the steeper transitions observed in the corresponding

(a)

(b)
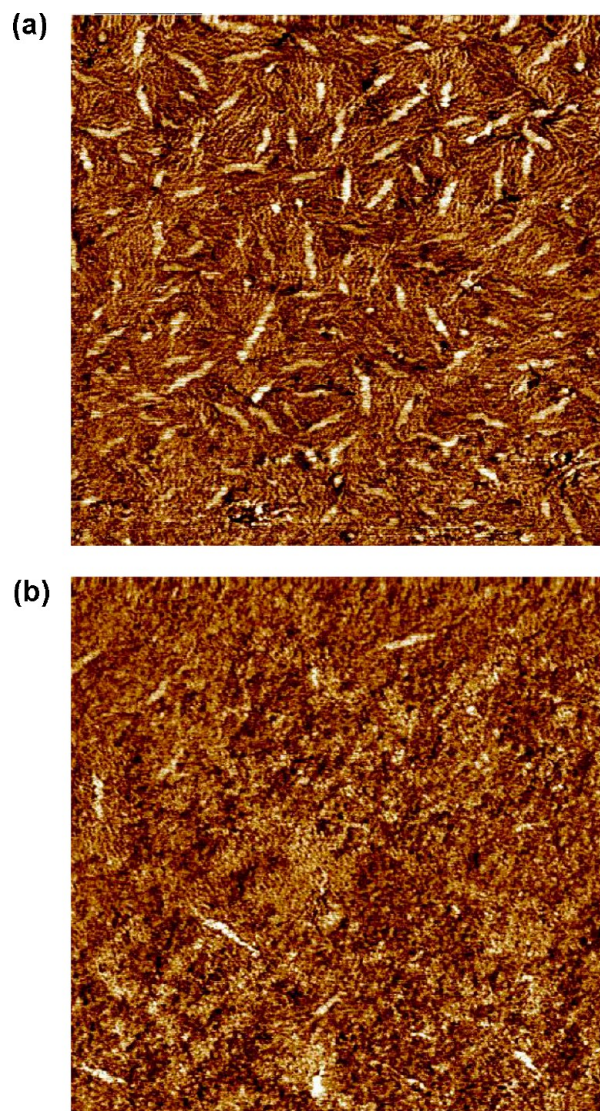
Figure 6. Tapping mode AFM phase images of HT98 P3HT films obtained by spin-coating from ultrasonicated solutions in CHCl$_3$: (a) without filtration and (b) after filtering the solutions through a 0.2 μm filter. The scan area is 2 × 2 μm^2.

(a)

(b)

Figure 7. (a) Solution-state and (b) solid-state absorption spectra of HT94 P3HT solutions in CHCl$_3$ and toluene and the corresponding films obtained by spin-coating them on to precleaned glass slides. Inset in b shows the solid-state absorption spectra of HT98 P3HT films obtained by spin-coating from cold and hot pristine solutions in *p*-xylene.

absorption spectra of the solutions upon irradiation, but also confirmed by reported thermochromic transitions.[35]

Here similar experiments performed using "marginal" solvents such as toluene or p-xylene (Figure 7(a)), revealed that the molecular aggregation process is dramatically accelerated resulting in spectroscopic changes that bear a close resemblance to those obtained by Zhao et.al. from high MW P3HT solutions . The spectroscopic changes noted in Figure 7a are significantly different from the results obtained from irradiation of P3HT in CHCl$_3$ solution, Figure 3a, highlighting the role played by the solvent system. Two essential differences must be noted in the case of ultrasonic irradiation of HT94 P3HT solutions in toluene for the same irradiation time (2 min): (i) the absorption maximum, $\lambda_{max,}$ is red-shifted by ca. 8 nm and (ii) the low energy transitions at ca. 555 and 603 nm are more intense. Clearly, solubility effects have a role in the ultrasound induced ordering phenomenon. In fact, irradiation for longer times (>2 min) followed by allowing the P3HT/toluene (or xylene) solution to rest for a few minutes, leads to the formation of a gel-like substance,

consistent with the reports of Malik et.al. who have demonstrated thermoreversible gel formation in P3HT/xylene systems.[40] The spectral features present in Figure 7 suggest that ultrasonic irradiation drives a random coil to rod transformation as evidenced by the bathochromic shift of the absorption maximum, followed by aggregation of the rods or fibrillar crystallization.[40,41] In addition, there are distinct similarities in spectral features of the irradiated toluene solutions (Figure 7) and thermochromic transitions occurring in P3HT solution observed by Rughooputh et.al., supporting the concept of an ultrasound induced coil−rod transformation driving the crystallization process.[41]

Kiriy et.al. suggested that the addition of nonsolvents to well dissolved P3HT solutions leads to solvophobic interactions that result in main chain collapse into a helical conformation followed by a concentration dependent association of individual helices into one-dimensional aggregates.[42] However, as noted above, the significant differences in the spectral features observed for irradiated CHCl$_3$ vs toluene solutions of the π-conjugated polymer indicate that the development of nano/microcrystalline aggregates is fundamentally different in the two systems. Figure 7b compares the solid-state spectra obtained by spin-coating toluene and CHCl$_3$ HT94 P3HT solutions. Considering the discussion above, it appears that ultrasonic

2375

dx.doi.org/10.1021/am3027822 | ACS Appl. Mater. Interfaces 2013, 5, 2368−2377

irradiation of solutions of P3HT in marginal solvents provides for increased molecular order in the solid state. This increased order is not mirrored in the corresponding field effect mobilities, with values of ca. 2×10^{-3} cm^2 V^{-1} s^{-1} and 2×10^{-2} cm^2 V^{-1} s^{-1} obtained from devices prepared by spin-coating irradiated solutions of HT94 P3HT in toluene and CHCl$_3$, respectively. The inset in Figure 7b shows the solid state spectra of HT98 P3HT obtained by spin-coating from both, a hot solution in p-xylene and one that was allowed to cool to room temperature. As evidenced by the differences observed in the absorption spectra, p-xylene is also a marginal solvent for P3HT and the reduced solubility results in increased aggregation among the polymer chains.

Additional experiments using methanol (MeOH) to deliberately aggregate HT94 P3HT/CHCl$_3$ solutions in a controllable manner, reveal that mobility as a function of MeOH vol % initially increases leading up to a peak mobility, followed by a sharp decrease upon further increase in MeOH content. The existence of a peak mobility distinctly points to the sensitivity of charge transport to the nature or physical conformation of the aggregate formed in solution, which is expected to evolve as MeOH vol % increases (see the Supporting Information for a detailed description of the MeOH aggregation experiments). These results suggest that charge transport through the network of ordered aggregates formed in the ultrasonicated solution depends on the "physical conformation" of the polymer chains within those aggregates, and is thus dependent on the existing polymer/solvent interactions. Ultrasonic irradiation of solutions of HT94 P3HT in monochlorobenzene (MCB) show none of the spectroscopic changes observed for either CHCl$_3$ or toluene solutions, even upon irradiation for 20 min (see the Supporting Information), confirming the role of solubility effects on the ultrasound induced aggregation process. This is consistent with the results of the MeOH aggregation experiments, which suggest that the solubility of P3HT in the solvents studied is in the order MCB > CHCl$_3$ > toluene.

The effect of RR can also be understood in light of the solubility effects discussed above. The more planar and rigid chain conformation in HT98 P3HT, afforded by fewer steric distortions imposed by the hexyl side chains, is expected to lead to a lower solubility in a given solvent relative to the lower RR counterpart, HT94 P3HT. The fact that the HT98 solutions are routinely more sensitive to ultrasonic irradiation in spite of the lower molecular weight of this material compared to HT94 (see Table 1), suggests that RR has a dominant influence on the polymer solubility. Disentanglement of the polymer chains resulting from ultrasonic irradiation, leads to the formation of molecular aggregates, the nature of which depend upon the solvent environment surrounding the disentangled chains and polymer RR, both of which explain the differences noted in the absorption spectra reported earlier. Regiorandom P3HT with a H-T content of ca. 50% is unresponsive to ultrasonic irradiation (see the Supporting Information). The decrease in sensitivity of the π-conjugated polymer to ultrasonic irradiation with decreasing RR suggests that the ultrasonication conditions (40 kHz, 130 W) may be too mild to surmount the large steric barrier in less regioregular polymers, preventing efficient cofacial π stacking. The experiments described here further confirm that the nature of the aggregates plays a dominant role in dictating charge transport through the π-conjugated polymer films. Ultrasonic irradiation exploits solvent−solute interactions, which are crucial to the formation of these aggregates and thus impact the corresponding macroscale charge carrier mobility.

CONCLUSIONS

Overall, the results presented here show a balance between intrinsic RR effects and extrinsic effects, film deposition conditions, in particular. In the lower RR P3HT sample, HT94, which does not benefit from the high degree of intrachain ordering, the mobility scales with both the improvement in thin-film morphology as well as the intensity of the XRD peaks. In other words, techniques that result in improved nano/microstructural quality (e.g., dip-coating and ultrasonication) provide for consequential improvement in charge transport. However, this correlation is not found in the case of the higher RR variant. The higher RR affords an inherently higher degree of intrachain ordering, which in and of itself provides for more facile charge transport. As a result, any further improvement in thin film microstructure only leads to minor changes in charge transport as determined by field effect mobility. We suggest that because multiple pathways for charge transport (intra- vs interchain) are evident, the role of morphology in dictating macroscopic field effect mobility is highly sensitive to the balance between intra- and interchain ordering, and thus to the total system in which it is studied. As our results pertaining to the role of solvent suggest, improved understanding of the complex nano/microstructure−charge transport correlation can only be achieved through a detailed analysis of the physical conformation of the polymer chains within the crystallized aggregates, a subject that requires further investigation. The relationships between molecular and process parameters are demonstrated to be very subtle: modulation of one effects changes in the others, which in turn impact charge transport on the macroscale. The results presented here provide insight into the degree of control that is required for the development of reproducible, robust materials and processes for advanced flexible electronics based on polymeric materials.

ASSOCIATED CONTENT

ⓢ Supporting Information

The results of fits to the UV−vis spectra, P3HT filtration experiments, output characteristics of P3HT OFETs under a variety of conditions, effect of dielectric surface modification, and methanol aggregation experiments are discussed. This material is available free of charge via the Internet at http://pubs.acs.org/.

AUTHOR INFORMATION

Corresponding Author
*E-mail: ereichmanis@chbe.gatech.edu.

Notes
The authors declare no competing financial interest.

ACKNOWLEDGMENTS

REFERENCES

(1) Mei, J.; Kim, D. H.; Ayzner, A. L.; Toney, M. F.; Bao, Z. *J. Am. Chem. Soc.* **2011**, *133*, 20130.

2376

dx.doi.org/10.1021/am3027822 | ACS Appl. Mater. Interfaces 2013, 5, 2368−2377

(2) Sirringhaus, H.; Tessler, N.; Friend, R. H. *Science* **1998**, *280*, 1741.

(3) Robert, A. S. *Adv. Mater.* **2009**, *21*, 2007.

(4) Chang, J.-F.; Clark, J.; Zhao, N.; Sirringhaus, H.; Breiby, D. W.; Andreasen, J. W.; Nielsen, M. M.; Giles, M.; Heeney, M.; McCulloch, I. *Phys. Rev. B* **2006**, *74*, 115318.

(5) Kline, R. J.; McGehee, M. D.; Kadnikova, E. N.; Liu, J.; Fréchet, J. M. J. *Adv. Mater.* **2003**, *15*, 1519.

(6) Chang, J. F.; Sun, B.; Breiby, D. W.; Nielsen, M. M.; Solling, T. I.; Giles, M.; McCulloch, I.; Sirringhaus, H. *Chem. Mater.* **2004**, *16*, 4772.

(7) Hoichang, Y.; Scott, W. L.; Chang, Y. R.; Zhenan, B. *Appl. Phys. Lett.* **2007**, *90*, 172116.

(8) Kim, D. H.; Park, Y. D.; Jang, Y.; Yang, H.; Kim, Y. H.; Han, J. I.; Moon, D. G.; Park, S.; Chang, T.; Chang, C.; Joo, M.; Ryu, C. Y.; Cho, K. *Adv. Funct. Mater.* **2005**, *15*, 77.

(9) Aiyar, A. R.; Hong, J.-I.; Nambiar, R.; Collard, D. M.; Reichmanis, E. *Adv. Funct. Mater.* **2011**, *21*, 2652.

(10) Wang, G.; Hirasa, T.; Moses, D.; Heeger, A. J. *Synth. Met.* **2004**, *146*, 127.

(11) Sirringhaus, H.; Brown, P. J.; Friend, R. H.; Nielsen, M. M.; Bechgaard, K.; Langeveld-Voss, B. M. W.; Spiering, A. J. H.; Janssen, R. A. J.; Meijer, E. W.; Herwig, P. *Nature* **1999**, *401*, 685.

(12) Zhenan, B.; Ananth, D.; Andrew, J. L. *Appl. Phys. Lett.* **1996**, *69*, 4108.

(13) Surin, M.; Leclere, P.; Lazzaroni, R.; Yuen, J. D.; Wang, G.; Moses, D.; Heeger, A. J.; Cho, S.; Lee, K. *J. Appl. Phys.* **2006**, *100*, 033712.

(14) Ho, P. H.; Chua, L. L.; Dipankar, M.; Gao, X.; Qi, D.; Wee, A. S.; Chang, J. F.; Friend, R. *Adv. Mater.* **2007**, *19*, 215.

(15) Kim, D. H.; Jang, Y.; Park, Y. D.; Cho, K. *Macromolecules* **2006**, *39*, 5843.

(16) Cho, S.; Lee, K.; Yuen, J.; Wang, G.; Moses, D.; Heeger, A. J.; Surin, M.; Lazzaroni, R. *J. Appl. Phys.* **2006**, *100*, 114503.

(17) Mattis, B. A.; Chang, P. C.; Subramanian, V. *Synth. Met.* **2006**, *156*, 1241.

(18) Coropceanu, V.; Cornil, J.; da Silva Filho, D. A.; Olivier, Y.; Silbey, R.; Bredas, J. L. *Chem. Rev* **2007**, *107*, 926.

(19) Jenny, C.; Jui-Fen, C.; Frank, C. S.; Richard, H. F.; Carlos, S. *Appl. Phys. Lett.* **2009**, *94*, 163306.

(20) Street, R. A.; Northrup, J. E.; Salleo, A. *Phys. Rev. B* **2005**, *71*, 165202.

(21) Chabinyc, M. L. *Polym. Rev.* **2008**, *48*, 463.

(22) Pierret, R. F. *Field Effect Devices*; Prentice Hall: Upper Saddle River, NJ, 1990.

(23) Brédas, J.-L.; Beljonne, D.; Coropceanu, V.; Cornil, J. *Chem. Rev.* **2004**, *104*, 4971.

(24) Volkel, A. R.; Street, R. A.; Knipp, D. *Phys. Rev. B* **2002**, *66*, 195336.

(25) Sirringhaus, H.; Tessler, N.; Thomas, D.; Brown, P.; Friend, R. In *Advances in Solid State Physics 39*; Kramer, B., Ed.; Springer: Berlin, 1999; Vol. 39, p 101.

(26) Chua, L.-L.; Zaumseil, J.; Chang, J.-F.; Ou, E. C. W.; Ho, P. K. H.; Sirringhaus, H.; Friend, R. H. *Nature* **2005**, *434*, 194.

(27) Hao, X. T.; Hosokai, T.; Mitsuo, N.; Kera, S.; Okudaira, K. K.; Mase, K.; Ueno, N. *J. Phys. Chem. B* **2007**, *111*, 10365.

(28) Sandberg, H. G. O.; Frey, G. L.; Shkunov, M. N.; Sirringhaus, H.; Friend, R. H.; Nielsen, M. M.; Kumpf, C. *Langmuir* **2002**, *18*, 10176.

(29) Dodabalapur, A.; Torsi, L.; Katz, H. E. *Science* **1995**, *268*, 270.

(30) Clark, J.; Silva, C.; Friend, R. H.; Spano, F. C. *Phys. Rev. Lett.* **2007**, *98*, 206406.

(31) Spano, F. C. *Chem. Phys.* **2006**, *325*, 22.

(32) Brown, P. J.; Thomas, D. S.; Kohler, A.; Wilson, J. S.; Kim, J.-S.; Ramsdale, C. M.; Sirringhaus, H.; Friend, R. H. *Phys. Rev. B* **2003**, *67*, 064203.

(33) Nguyen, T. Q.; Yee, R. Y.; Schwartz, B. J. *J. Photochem. Photobiol., A* **2001**, *144*, 21.

(34) Amrutha, S. R.; Jayakannan, M. *J. Phys. Chem. B* **2006**, *110*, 4083.

(35) Zhao, K.; Xue, L.; Liu, J.; Gao, X.; Wu, S.; Han, Y.; Geng, Y. *Langmuir* **2009**, *26*, 471.

(36) Wang, G.; Swensen, J.; Moses, D.; Heeger, A. J. *Increased Mobility from Regioregular Poly(3-Hexylthiophene) Field-Effect Transistors*; American Institute of Physics: College Park, MD, 2003; Vol. 93.

(37) Ihn, K. J.; Moulton, J.; Smith, P. *J. Polym. Sci., Part B: Polym. Phys.* **1993**, *31*, 735.

(38) Prosa, T. J.; Winokur, M. J.; Moulton, J.; Smith, P.; Heeger, A. J. *Macromolecules* **1992**, *25*, 4364.

(39) Aiyar, A. R.; Hong, J.-I.; Reichmanis, E. *Chem. Mater.* **2012**, *24*, 2845.

(40) Malik, S.; Jana, T.; Nandi, A. K. *Macromolecules* **2000**, *34*, 275.

(41) Rughooputh, S.; Hotta, S.; Heeger, A. J.; Wudl, F. *J. Polym. Sci., Part B: Polym. Phys.* **1987**, *25*, 1071.

(42) Kiriy, N.; Jähne, E.; Adler, H. J.; Schneider, M.; Kiriy, A.; Gorodyska, G.; Minko, S.; Jehnichen, D.; Simon, P.; Fokin, A. A. *Nano Lett.* **2003**, *3*, 707.

2377

dx.doi.org/10.1021/am3027822 | *ACS Appl. Mater. Interfaces* 2013, 5, 2368–2377